Appendix A: Supplementary Material

Efficacy and Self-Similarity of SARS-CoV-2 Thermal Decontamination

Te Faye Yap[1,†], Jason C. Hsu[2,†], Zhen Liu[1], Kempaiah Rayavara[2], Vivian Tat[2], Chien-Te K. Tseng[2,3], and Daniel J. Preston[1,*]

[1]Department of Mechanical Engineering, George R. Brown School of Engineering, Rice University; 6100 Main St., Houston, TX 77005, USA.

[2]Department of Microbiology and Immunology, University of Texas Medical Branch; 301 University Blvd., Galveston, TX 77555, USA.

[3]Center for Biodefense and Emerging Disease, Galveston National Laboratory, University of Texas Medical Branch; 301 University Blvd., Galveston, TX 77555, USA.

[†]These authors contributed equally to this work

*Corresponding author. Email: djp@rice.edu

Supplementary Text

1. Statistical Analysis

1.1 Experimental Error Analysis

The experimental error for the concentration measurement at a given temperature can be determined from the standard deviation:

$$\sigma_{[C]} = \sqrt{\frac{1}{N-1}\sum_{i=1}^{N}([C_i] - [\bar{C}])^2} \quad \text{[Eq. S1]}$$

where N is the number of data points, $[C_i]$ is the experimental concentration, and $[\bar{C}]$ is the mean concentration for a given time point. To determine the corresponding error in the nondimensionalized concentration, $[C]^*$, the error is propagated based on the method of first partial derivatives:

$$\sigma_{[C]^*} = \sqrt{\left(\frac{\sigma_{[C]}}{[C_0]}\right)^2 + \left(\frac{[C]\cdot\sigma_{[C_0]}}{[C_0]^2}\right)^2} \quad \text{[Eq. S2]}$$

where σ represents the error associated with each measured quantity. This approach is used to determine the combined nondimensionalized error plotted in Figure 2. Error bars plotted on the nondimensionalized logarithmic plot (Figure 1B and 2A) were determined by propagating the error for the log base 10 of $[C]^*$ using the error determined from Eq. S2, shown here in Eq. S3:

$$\sigma_{\log_{10}[C]^*} = \log_{10} e \left(\frac{\sigma_{[C]^*}}{[C]^*}\right) \quad \text{[Eq. S3]}$$

1.2 Identification of Outliers

We nondimensionalized the experimental data from our work and prior work for SARS-CoV-2, SARS-CoV-1, and MERS-CoV, and plotted the data against our universal model in Figure 2 in the main text. To identify outlier points that deviate from the universal model, we evaluate the residuals, ε, of each experimental data point by taking the difference between the experimentally determined y-value (i.e., $\log_{10}[C]^*$) and the model y-value as shown in Eq. S4:

$$y - y_{model} = \varepsilon \quad \text{[Eq. S4]}$$

We determine the sum of squares for the error, SSE, using Eq. S5:

$$\sum_{i=1}^{n} \varepsilon^2 = SSE \quad \text{[Eq. S5]}$$

which is used to determine the standard deviation of the residuals, σ, for each virus dataset:

$$\sigma = \sqrt{\frac{SSE}{n-2}} \quad \text{[Eq. S6]}$$

Data points with residual magnitudes, |ε|, that are positive or greater than two times the standard deviation of the residuals, 2σ, are considered to be outlier data points (Illowsky and Dean, 2021). The two points indicated with arrows in Figure 2(B and D) have residuals greater than 2σ. Tables S1–4 show the values for the statistical parameters used to determine the outliers for each dataset in Figure 2. The outlier data points are bolded and labeled with an asterisk in the tables.

2. Procedure to Determine E_a and ln(A)

2.1. Data Visualization and Interpretation

The experimental data are plotted according to the linearized rate law for a first-order reaction (Eq. S7) as shown in Figure S1. The magnitude of the slope of the best fit line corresponds to the rate constant, k, at a given temperature, T.

$$ln\frac{[C]}{[C_0]} = -kt \quad \text{[Eq. S7]}$$

Each pair of (k, T) is plotted in Figure S2 according to the linearized Arrhenius equation (Eq. S8) and the values are tabulated in Table S5:

$$\ln(k) = -\frac{E_a}{RT} + ln(A) \quad \text{[Eq. S8]}$$

where R is the gas constant, E_a is the activation energy associated with inactivation for a given virus, and A is the frequency factor. The values of E_a and ln(A) for the SARS-CoV-2 virus can be determined by equating -E_a/R and ln(A) to the slope (Eq. S9) and intercept (Eq. S10) of the linear fit with the form of the linearized Arrhenius equation shown in Figure S2, respectively.

$$-\frac{E_a}{R\times 10^4} = slope \quad \text{[Eq. S9]}$$

$$\ln(A) = intercept \quad \text{[Eq. S10]}$$

The linear correlation between E_a and ln(A) for the range of coronaviruses shown in Figure S3 indicates that they undergo a thermal denaturation process following the Meyer-Neldel rule (Qin et al., 2014; Wright, 2003), which arises from entropy-enthalpy compensation. The E_a and ln(A) for SARS-CoV-2 determined in this work are plotted with the values for other coronaviruses determined in prior work; the

overlap indicates that the inactivation behavior is similar. The values of E_a and ln(A) for SARS-CoV-2 and the percentage differences between the values determined in this work and in a prior data-driven study (Yap et al., 2020) are tabulated in Table S6.

2.2. Inactivation Rate Model

The rate law for a first-order reaction (Eq. S7) and the Arrhenius equation (Eq. S8) were combined by substituting the Arrhenius equation, rearranged in terms of rate constant, into the expression for the rate law. We rearranged to generate an analytical model for the thermal decontamination time as a function of temperature (Eq. 1 in the main text).

2.3. Linearly-Scaled Experimental Data

The experimental results are plotted with linear axes in Figure S4 to provide an additional view from which to compare the decrease in concentration of viable virions versus time at four different temperatures (as opposed to the log axes used in the main text Figure 1B).

3. Procedure to Determine Relative Humidity at Elevated Temperatures

Relative humidity (RH) is the ratio of actual water vapor pressure or vapor density, ρ_{act}, in the air compared to the saturated vapor pressure or vapor density, $\rho_{sat,T}$, at a given temperature. Because the relative humidity depends on temperature, as we heat the samples in a closed oven with a fixed volume of air, the relative humidity will decrease. Taking the initial conditions of the ambient air temperature to be 25 °C and the relative humidity, $RH_{initial,\ 25\ °C}$ to be 50% (within our reported RH range), we can determine the actual water vapor density in the air using Eq. S11:

$$RH_{intial,25℃} = \frac{Actual\ vapor\ density, \rho_{act}}{Saturated\ vapor\ density\ at\ 25℃, \rho_{sat,25\ ℃}} \quad \text{[Eq. S11]}$$

Rearranging the terms to determine the ρ_{act}:

$$\rho_{act} = 50\% \times \rho_{sat,25℃} \quad \text{[Eq. S12]}$$

The $\rho_{sat,T}$ for a given temperature can be determined from fluid property tables for saturated water (Çengel and Boles, 2015). After the oven heats up to a given setpoint temperature, we can determine the new relative humidity in the oven at elevated temperatures (Eq. S13) using ρ_{act} determined from Eq. S12.

$$RH_{oven,T} = \frac{\rho_{act}}{Saturated\ vapor\ density\ at\ 25℃, \rho_{sat,70\ ℃}} \quad \text{[Eq. S13]}$$

The values of the parameters and the estimated relative humidity at each oven setpoint temperature are tabulated in Table S7. The estimated relative humidity value at 70 °C is in close agreement with relative humidity measurements of air inside a heated electric cooker measured using a thermo-hygrometer at 100 °C, which were reported as ~ 5% in prior work (Oh et al., 2020).

4. Degradation of Meltblown Filter Layer

Surgical masks were heated to elevated temperatures greater than those used for decontamination in our work, and SEM images were taken to illustrate the changes in physical morphology of heat-degraded meltblown filter layers. Prior work reported a decrease in filtration efficiency when heating the meltblown filter layer to 125 °C (Liao et al., 2020); using SEM imaging, we compare a sample heated to 125 °C (the reported temperature where degradation occurs) for 30 minutes in Figure S5A to an unheated sample in Figure 3B. We observe a change in the physical morphology due to relaxation of the crystalline structure as we increase the temperature close to the polymer's melting point (Campos et al., 2020). The material used in the meltblown filter layer (i.e., polypropylene) has typical melting points ranging from 130 °C to 170 °C. To further demonstrate the sensitivity of the meltblown layer morphology to high temperatures, we heated the filter layer to 150 °C (for 10 minutes), 155 °C (for 2 minutes), and 160 °C (for 2 minutes) and observed a significant change in the physical morphology and degradation of the filter layer (Figure S5B–D). This characterization method shows that typical dry heat decontamination temperatures (~160 °C) are not suitable for decontaminating delicate PPE (Darmady et al., 1961).

5. Transient Heating Period of Samples

We characterized the experimental temperature profile of a mask sample as it heated up in the oven to determine whether the transient heating period represented a significant source of error. We placed a mask sample on a preheated plate following the same procedure used in all of the experiments, and we recorded the temperature of the mask over time. We determined that the sample heats up to the setpoint temperature in approximately 30 seconds. We show the experimentally measured temperature profile of the mask sample being heat treated at 70 °C in Figure S6. The time required for the mask temperature to

reach the setpoint temperature, 70 °C, is ~10 % of the total time required to achieve a 3-log reduction of SARS-CoV-2 (5 minutes), which is the shortest decontamination duration studied in our work. For longer decontamination times and at lower temperatures, the percentage of the total time for the transient heating period is smaller, and it does not represent a significant source of error in any of our experiments.

Supplementary Figures

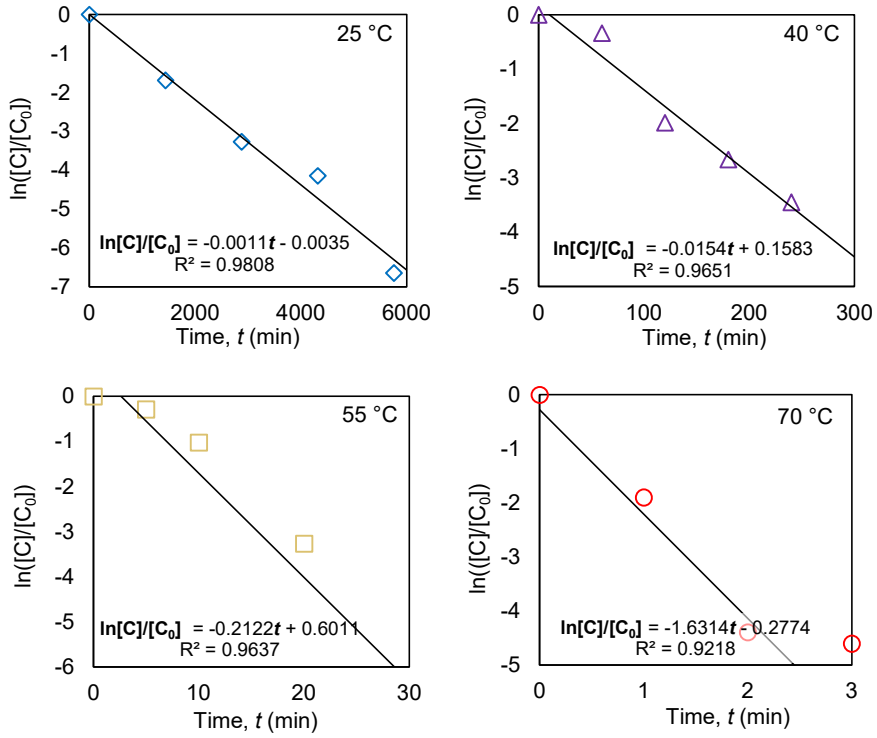

Figure S1. Primary data for inactivation of SARS-CoV-2 on surgical masks after converting the n-log reduction values from log base 10 to natural log. We fit a line according to Eq. S7 to the data to estimate the rate constants at 25 °C, 40 °C, 55 °C, and 70 °C.

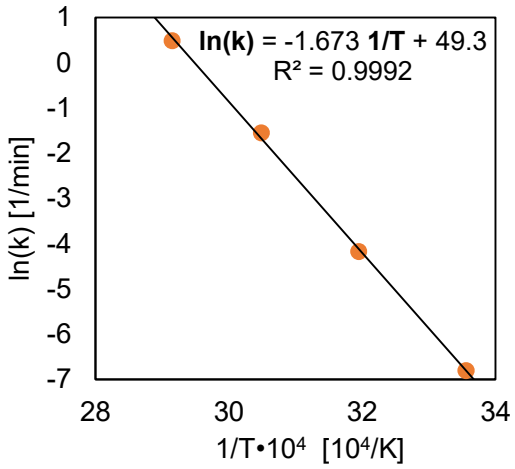

Figure S2. From the primary data, the rate constant, k, for a given temperature was determined using a linear regression according to Eq. S8. The slope and intercept of the linear fit correspond to the activation energy, E_a, and frequency factor, ln(A), for SARS-CoV-2.

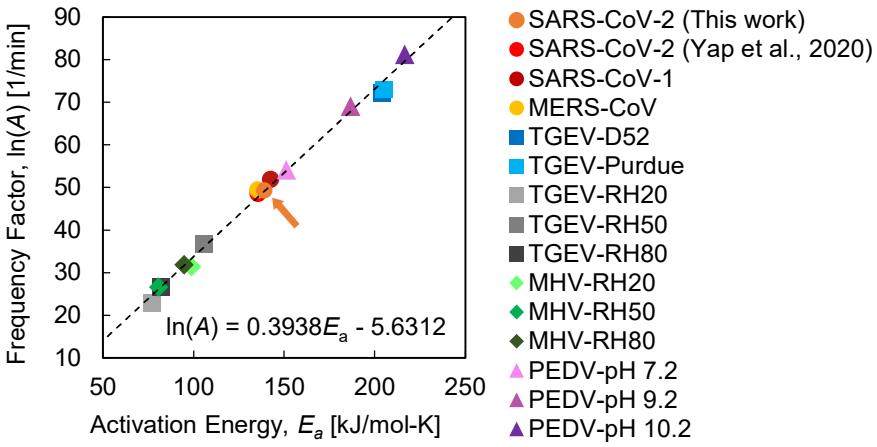

Figure S3. Thermal inactivation behavior of a range of coronaviruses, adapted from prior work (Yap et al., 2020) that applied a data-driven approach. The frequency factor, ln(A), is plotted against the activation energy, E_a, according to the Arrhenius equation; the linear relationship indicates protein denaturation. The E_a and ln(A) determined in this work (indicated by the arrow) are similar to the values determined in prior work for SARS-CoV-2 on a range of fomites.

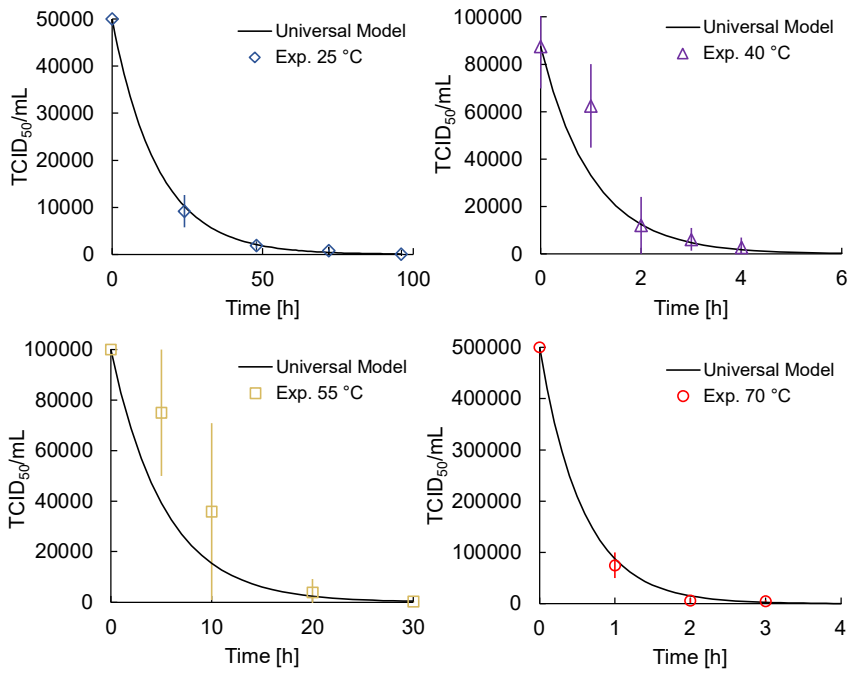

Figure S4. Experimental results obtained at 25 °C, 40 °C, 55 °C, and 70 °C show that the inactivation timescale for decontamination of SARS-CoV-2 on PPE spans more than three orders of magnitude (i.e., from less than 5 minutes to nearly 100 hours for a 3-log reduction corresponding to effective decontamination).

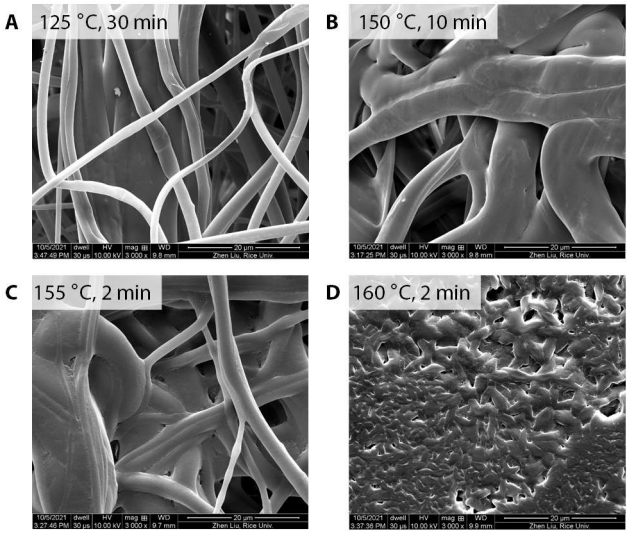

Figure S5. SEM images of the meltblown filter layer after dry heat treatment at (A) 125 °C for 30 minutes, (B) 150 °C for 10 minutes, (C) 155 °C for 2 minutes, and (D) 160 °C for 2 minutes.

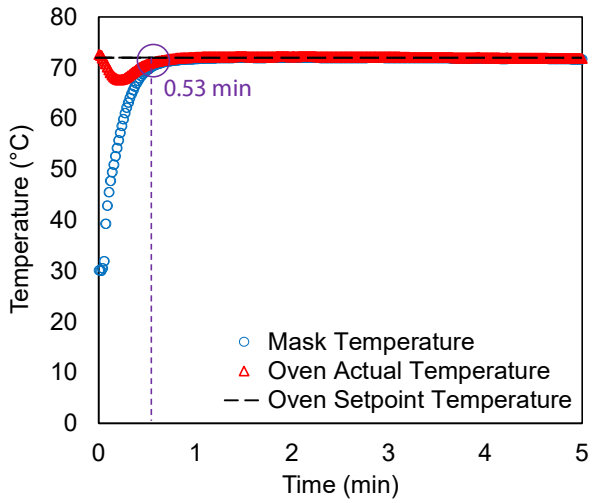

Figure S6. Temperature profile of a mask sample heated to 70 °C. The actual temperature in the oven dipped below the setpoint when the door of the oven was opened to load the sample, but the temperature quickly returned to the setpoint temperature after the door was closed. The mask sample temperature increased from room temperature initially (time = 0 min) to the oven setpoint in less than one minute.

Table S1. Statistical parameters used in determining the outliers for SARS-CoV-2 inactivation in this work.

T(°C)	t^*	$\log(C^*)_{exp.}$	$\varepsilon = \log(C^*)_{exp} - \log(C^*)_{model}$	ε^2	$\lvert \varepsilon \rvert - 2\sigma$
25	0	0	0.000	0.000	-0.445
25	0.708	- 0.737	-0.028	0.001	-0.417
25	1.417	- 1.420	-0.003	0.000	-0.441
25	2.125	- 1.800	0.325	0.106	-0.120
25	2.834	- 2.886	-0.052	0.003	-0.393
40	0	0	0.000	0.000	-0.445
40	0.434	- 0.146	0.288	0.083	-0.157
40	0.868	- 0.863	0.005	0.000	-0.440
40	1.302	-1.158	0.144	0.021	-0.301
40	1.736	-1.499	0.237	0.056	-0.208
55	0	0	0.000	0.000	-0.445
55	0.416	-0.125	0.291	0.085	-0.154
55	0.832	-0.446	0.386	0.149	-0.059
55	1.663	-1.416	0.247	0.061	-0.198
55	2.500	-2.699	-0.204	0.042	-0.241
70	0	0	0.000	0.000	-0.445
70	0.772	-0.824	-0.051	0.003	-0.393
70	1.545	-1.909	-0.364	0.132	-0.081
70	2.317	-2	0.317	0.101	-0.127
				SSE = 0.841	σ = 0.222

Table S2. Statistical parameters used in determining the outliers for SARS-CoV-2 inactivation in prior work (Chin et al., 2020; van Doremalen et al., 2020).

T(°C)	t^*	$\log(C^*)_{exp.}$	$\varepsilon = \log(C^*)_{exp} - \log(C^*)_{model}$	ε^2	$\lvert \varepsilon \rvert - 2\sigma$
20	0	0	0	0	-1.241
20	0.022	-0.420	-0.398	0.159	-0.843
20	0.087	-0.440	-0.353	0.124	-0.888
20	0.174	-0.590	-0.416	0.173	-0.825
20	0.523	-1.110	-0.587	0.344	-0.654
20	**1.047**	**-2.330**	**-1.283**	**1.647**	**0.043***
22	0	0	0	0	-1.241
22	0.008	-0.030	-0.022	0.000	-1.219
22	0.050	-0.670	-0.620	0.384	-0.621
22	0.100	-0.810	-0.710	0.504	-0.531
22	0.400	-1.050	-0.650	0.422	-0.591
22	0.801	-1.580	-0.779	0.607	-0.462
22	1.602	-2.070	-0.468	0.219	-0.773
22	2.803	-2.990	-0.187	0.035	-1.054
				SSE = 4.619	σ = 0.620

Table S3. Statistical parameters used in determining the outliers for SARS-CoV-1 inactivation in prior work (Darnell and Taylor, 2006; van Doremalen et al., 2020).

T(°C)	t^*	$\log(C^*)_{exp.}$	$\varepsilon = \log(C^*)_{exp} - \log(C^*)_{model}$	ε^2	$\lvert \varepsilon \rvert - 2\sigma$
22	0	0	0	0	-0.545
22	0.051	-0.390	-0.339	0.115	-0.206
22	0.203	-0.320	-0.117	0.014	-0.429
22	0.407	-0.760	-0.353	0.125	-0.192
22	1.220	-1.480	-0.260	0.068	-0.285
22	2.440	-2.540	-0.100	0.010	-0.445
56	0	0	0	0	-0.545
56	3.462	-3.959	-0.497	0.247	-0.049
65	0	0	0.000	0	-0.545
65	1.336	-1.205	0.131	0.017	-0.414
				SSE = 0.595	σ = 0.273

Table S4. Statistical parameters used in determining the outliers for MERS-CoV inactivation in this work (Leclercq et al., 2014; van Doremalen et al., 2013).

T(°C)	t^*	$\log(C^*)_{exp.}$	$\varepsilon = \log(C^*)_{exp} - \log(C^*)_{model}$	ε^2	$\lvert \varepsilon \rvert - 2\sigma$
20	0.000	0.000	0.000	0.000	-1.311
20	0.010	0.132	0.142	0.020	-1.169
20	0.029	-0.538	-0.509	0.259	-0.802
20	0.235	-0.560	-0.325	0.105	-0.986
20	0.471	-1.021	-0.551	0.303	-0.760
20	1.412	-1.416	-0.004	0.000	-1.307
20	**2.824**	**-4.326**	**-1.502**	**2.256**	**0.191***
20	4.236	-4.714	-0.478	0.229	-0.833
56	0.000	0.000	0.000	0.000	-1.311
56	0.214	-0.090	0.124	0.015	-1.186
56	0.214	0.580	0.794	0.631	-0.516
56	0.214	-0.920	-0.706	0.498	-0.605
65	0.000	0.000	0.000	0.000	-1.311
65	0.801	-0.920	-0.119	0.014	-1.192
65	0.801	-1.920	-1.119	1.252	-0.192
				SSE = 5.582	σ = 0.655

Table S5. The rate constant, k, at each experimental temperature determined from Figure S1 and plotted in Figure S2.

Temperature [°C]	$1/T \bullet 10^4$ [10^4/K]	k [1/min]	ln(k)
25	33.56	0.0011	- 6.812
40	31.95	0.0154	- 4.173
55	30.49	0.2122	-1.550
70	29.15	1.6314	0.489

Table S6. The frequency factor, ln(A), and activation energy, E_a, for SARS-CoV-2 determined from the present experimental work and from a data-driven approach used in prior work (Yap et al., 2020).

	Frequency factor, ln(A) [1/min]	Activation energy, E_a [kJ/mol]
Present work	49.3	139.1
Prior data-driven approach (Yap et al., 2020)	48.6	135.7
Percent difference (%)	1.46	2.48

Table S7. Values used to estimate the relative humidity at different oven setpoint temperatures.

T (°C)	$\rho_{sat.\ T}$ (kg/m^3)	RH (%).
25	0.0231	50
40	0.0512	23
55	0.1045	11
70	0.1984	6

Supplementary References

Campos, R.K., Jin, J., Rafael, G.H., Zhao, M., Liao, L., Simmons, G., Chu, S., Weaver, S.C., Chiu, W., Cui, Y., 2020. Decontamination of SARS-CoV-2 and other RNA viruses from N95 level meltblown polypropylene fabric using heat under different humidities. ACS Nano 14, 14017−14025. https://doi.org/10.1021/acsnano.0c06565

Çengel, Y. a., Boles, M.A., 2015. Thermodynamics: An Engineering Approach, 8th ed, McGraw-Hill. McGraw Hill Education.

Chin, A.W.H., Chu, J.T.S., Perera, M.R.A., Hui, K.P.Y., Yen, H.-L., Chan, M.C.W., Peiris, M., Poon, L.L.M., 2020. Stability of SARS-CoV-2 in different environmental conditions. The Lancet Microbe 1, e10. https://doi.org/10.1016/S2666-5247(20)30003-3

Darmady, E.M., Hughes, K.E., Jones, J.D., Prince, D., Tuke, W., 1961. Sterilization by dry heat. J. Clin. Pathol. 14, 38–44. https://doi.org/10.1136/jcp.14.1.38

Darnell, M.E.R., Taylor, D.R., 2006. Evaluation of inactivation methods for severe acute respiratory syndrome coronavirus in noncellular blood products. Transfusion 46, 1770–1777. https://doi.org/10.1111/j.1537-2995.2006.00976.x

Illowsky, B., Dean, S., 2021. Outliers [WWW Document]. URL https://stats.libretexts.org/@go/page/802 (accessed 10.7.21).

Leclercq, I., Batéjat, C., Burguière, A.M., Manuguerra, J.C., 2014. Heat inactivation of the Middle East respiratory syndrome coronavirus. Influenza Other Respi. Viruses. https://doi.org/10.1111/irv.12261

Liao, L., Xiao, W., Zhao, M., Yu, X., Wang, H., Wang, Q., Chu, S., Cui, Y., 2020. Can N95 respirators be reused after disinfection? And for how many times? ACS Nano 14, 6348–6356. https://doi.org/10.1021/acsnano.0c03597

Oh, C., Araud, E., Puthussery, J. V., Bai, H., Clark, G.G., Wang, L., Verma, V., Nguyen, T.H., 2020. Dry heat as a decontamination method for n95 respirator reuse. Environ. Sci. Technol. Lett. 7, 677–682. https://doi.org/10.1021/acs.estlett.0c00534

Qin, Z., Balasubramanian, S.K., Wolkers, W.F., Pearce, J.A., Bischof, J.C., 2014. Correlated Parameter Fit of Arrhenius Model for Thermal Denaturation of Proteins and Cells. Ann. Biomed. Eng. https://doi.org/10.1007/s10439-014-1100-y

van Doremalen, N., Bushmaker, T., Morris, D.H., Holbrook, M.G., Gamble, A., Williamson, B.N.,

Tamin, A., Harcourt, J.L., Thornburg, N.J., Gerber, S.I., Lloyd-Smith, J.O., de Wit, E., Munster, V.J., 2020. Aerosol and Surface Stability of SARS-CoV-2 as Compared with SARS-CoV-1. N. Engl. J. Med. https://doi.org/10.1056/NEJMc2004973

van Doremalen, N., Bushmaker, T., Munster, V.J., 2013. Stability of middle east respiratory syndrome coronavirus (MERS-CoV) under different environmental conditions. Eurosurveillance 18, 1–4. https://doi.org/10.2807/1560-7917.ES2013.18.38.20590

Wright, N.T., 2003. On a relationship between the Arrhenius parameters from thermal damage studies. J. Biomech. Eng. 125, 300–304. https://doi.org/10.1115/1.1553974

Yap, T.F., Liu, Z., Shveda, R.A., Preston, D.J., 2020. A predictive model of the temperature-dependent inactivation of coronaviruses. Appl. Phys. Lett. 117. https://doi.org/10.1063/5.0020782